Available online at www.sciencedirect.com
SCIENCE DIRECT®
Journal of Nuclear Materials 336 (2005) 31–39
journal of nuclear materials
www.elsevier.com/locate/jnucmat

Change in flow stress and ductility of δ-phase Pu–Ga alloys due to self-irradiation damage

A. Arsenlis *, W.G. Wolfer, A.J. Schwartz

Materials Science and Technology Division, Lawrence Livermore National Laboratory, University of California, P.O. Box 808, L-371 Livermore, CA 94551, USA

Received 7 August 2004; accepted 24 August 2004

Abstract

An internal state variable model for the mechanical behavior of aged Pu–Ga alloys is developed and used to predict the change of the material with accumulated self-irradiation damage or age. The material model incorporates microstructural data such as the primary irradiation-induced defect density from cascades, the density and average size of helium bubbles, the initial dislocation density, and the initial average segment length of the dislocation density as input parameters, and then evaluates the stress–strain response of a representative volume element of the material. Given this response at a single material point, the deformation behavior of tensile specimens is predicted, and it forecasts increased strength, decreased strain hardening, and more strain localization with aging. Although the material point behavior showed some slight strain softening, this strain softening is expected to be masked by statistical variations of different volume elements and by the strain rate sensitivity of the material. Hence, it is not expected to appear in the stress–strain response of macroscopic tensile specimens, and only the increase in flow stress will be measured.

1. Introduction

The change in the mechanical behavior of plutonium-based alloys with self-irradiation damage is of significant interest for the US Nuclear Stockpile Stewardship Program. Plutonium-based alloys, unlike other metal alloys, self-irradiate by alpha decay of plutonium at an estimated rate of 0.1 dpa per year [1]. Although the dose rate may not appear very high relative to dose rates in reactor materials, the integrated effect over decades may produce a significant density of nanometer scale defects due to self-irradiation, and lead to so-called 'aging' of the plutonium alloys. The self-irradiation induced defects come in the form of vacancies, vacancy clusters, voids, and helium bubbles, and their relative rates of production are strong functions of the irradiation conditions, namely of dose rate, temperature, time, microstructure, etc.

In this paper, we will focus on the plastic deformation properties of δ-phase Pu–Ga alloys at room temperature and the changes produced by accumulated irradiation-induced defects from the radioactive decay of plutonium. The δ-phase is face-centered-cubic, and it is the chosen Pu alloy structure because of its malleability at ambient conditions, in contrast to unalloyed

* Corresponding author. Tel.: +1 925 4242584; fax: +1 925 4237040.
E-mail address: arsenlis@llnl.gov (A. Arsenlis).

0022-3115/$ - see front matter © 2004 Elsevier B.V. All rights reserved.
doi:10.1016/j.jnucmat.2004.08.017

α-phase Pu, which is monoclinic and quite brittle. In this paper, we will extend recent advances in modeling the mechanical behavior of irradiated copper [2] and apply them to these plutonium alloys. We will utilize experimentally and theoretically determined parameters for the irradiation-induced defects and for the dislocation structure, and proceed to predict the mechanical behavior of these alloys using those gross features as input parameters.

In developing the model, we will rely heavily on the MTS model developed by Stout et al. for un-aged Pu–Ga alloys [3], and we will make appropriate modifications to the strain hardening to include the effects of the dominant irradiation-induced defects on the mechanical response. Several simplifying assumptions will also be made, such as material isotropy and consolidation of all the densities of the various irradiation induced defects into two representative densities. This will reduce substantially the complexity of the model while retaining the crucial physical aspects of more complex models that might be employed when more detailed microstructural characterization becomes available for aged Pu–Ga alloys. The present model will be used only to predict the behavior of a representative volume element of these alloys, but these predictions will be offered to approximate the changes expected in actual tensile specimen when texture, grain size variations, impurity content, and other heterogeneities can be neglected.

2. Constitutive model description

This isotropic constitutive model for self-irradiated δ-phase stabilized Pu–Ga alloys is based on the dispersed barrier hardening (DBH) models that have been previously applied to correlate the change in the yield strength of irradiated metals [4–7] and from concepts in dislocation density-based crystal plasticity models that have been used to capture the behavior of unirradiated fcc crystals [8,9]. The irradiation damage will be introduced into the model such that it reduces the mobility of the dislocation density, and we will assume that the irradiation-induced defect microstructure does not evolve with plastic deformation. The plastic behavior of the irradiated metal is determined by the evolution of a set of internal state variables for the total dislocation density, ρ_d; the average dislocation line segment length, $\bar{l}_d$; the current stress state, and the irradiation induced defect microstructure.

Microstructural investigations of aged Pu–Ga alloys show that the primary defects that accumulate with self-irradiation are nanometer scale helium bubbles [10]. Although dislocation loops have not been observed in Pu–Ga alloys, they are presumed to be present as remnants of the large collision cascades generated by the uranium recoil nuclei. Their presence has both been predicted by ion irradiation of lead and subsequently observed in transmission electron microscopy examinations [11].

Therefore, the irradiation-induced defect structure will be represented by the number density of dislocation loops, N_l, and their average size, d_l; as well as the number density of helium bubbles, N_b, and their average size, R_b. The forms of a majority of the constitutive equations and their material parameters were borrowed from the MTS model of δ-phase stabilized Pu–Ga alloys developed by Stout et al. [3] However, the effect of self-irradiation and the development of irradiation induced microstructure on the mechanical strength was outside the scope of Stout's MTS model. Therefore, the strain hardening portion of the model was changed from a strength-based to a dislocation density-based internal state variable model to facilitate the incorporation of the irradiation induced defects and their effects on the mechanical behavior of the material.

The basic structure of our framework is built from the finite deformation constitutive equations for isotropic hyperelastic–viscoplastic solids developed by Weber and Anand [12]. The framework consists of a multiplicative decomposition of the total deformation gradient into elastic and plastic parts and a classical J_2 flow theory with a normality flow condition and isotropic hardening defined in the intermediate, plastically deformed and elastically-relaxed, material configuration. With these considerations, the general three-dimensional model is simplified into a one dimensional theory governed by a set of scalar quantities. The constitutive equations that must be specified take the general form:

$$\dot{\bar{\varepsilon}}^p = f(\bar{\sigma}, \xi) \quad \text{and} \quad \dot{\xi} = g(\bar{\sigma}, \xi), \tag{1}$$

where $\dot{\bar{\varepsilon}}^p$ is the effective plastic strain rate, $\bar{\sigma}$ is an effective stress measure defined as the von Mises stress of the 2nd Piola–Kirchhoff stress in a plastically-deformed elastically-relaxed material configuration, and ξ is a set of internal state variables that quantify the current material state. In this case, the material defect densities and their representative lengths compose the set of internal state variables.

We will limit our considerations to loading conditions under ambient pressure, low strain rates, and low homologous temperatures such that we can assume that dislocation glide will be the dominant mechanism of plastic deformation, and the strain hardening will be controlled by the interactions of an evolving microstructure with the glissile dislocation density. Focusing first on the dislocation density, its complex and evolving structure will be represented by a scalar dislocation density measure, ρ_d, with units of length per unit volume and an average dislocation segment length, $\bar{l}_d$. A coarse-grained version of Orowan's equation will be

used to relate glide of the dislocation density to the effective plastic strain rate

$$\dot{\bar{\varepsilon}}^{\mathrm{p}} = \rho_{\mathrm{d}} b \bar{v}_{\mathrm{d}}, \tag{2}$$

where b is the magnitude of the Burgers vector, and $\bar{v}_{\mathrm{d}}$ is the average dislocation glide velocity. In this version of Orowan's equation, ρ_{d} is the total dislocation density, and $\bar{v}_{\mathrm{d}}$ is the average velocity of the total density including dislocation density that may be considered 'immobile' at the current stress level. The model does not explicitly distinguish between a 'mobile' and 'immobile' dislocation density, but rather assumes that the fraction of 'mobile' to 'immobile' dislocation density can be effectively incorporated into the expression for the average velocity. The evolution of the dislocation density with plastic deformation follows the form:

$$\dot{\rho}_{\mathrm{d}} = \left(\frac{2}{b\bar{l}_{\mathrm{d}}} - \rho_{\mathrm{d}}\frac{R_{\mathrm{c}}}{2b}\right)\dot{\bar{\varepsilon}}^{\mathrm{p}}, \tag{3}$$

$$\dot{\bar{l}}_{\mathrm{d}} = \left(\frac{\bar{l}_{\mathrm{d}}}{\rho_{\mathrm{d}}} - \delta\bar{l}_{\mathrm{d}}^{3}\right)\dot{\rho}_{\mathrm{d}}, \tag{4}$$

where R_{c} is the critical capture radius of annihilation, and δ is the dislocation line multiplication constant. The evolution equation for the dislocation density derives from the work of Essmann and Rapp [13], and the evolution equation for the average dislocation segment length derives from the work of Arsenlis and Tang [14].

To close the set of equations of the model, a constitutive function for the average velocity of the dislocation density, $\bar{v}_{\mathrm{d}}$, must be specified. This function must depend on the current stress and the current material state, as represented by the selection of internal state variables in the model. For the constitutive form of $\bar{v}_{\mathrm{d}}$, we rely heavily on the work of Stout et al. [3] who developed an MTS model for mechanical behavior of unirradiated δ-phase stabilized Pu–Ga alloys. In their strength-based MTS model, they define a closed form expression for the effective plastic strain rate as a function of the effective stress measure and a list of strength-based internal state variables. In this treatment, we have incorporated the functional dependencies found in their effective plastic strain rate expression into our expression for the average dislocation velocity. The resulting form for $\bar{v}_{\mathrm{d}}$ becomes

$$\bar{v}_{\mathrm{d}} = v_0 \exp\left[-\frac{\Delta F}{k\theta}\left(1 - \left(\frac{\bar{\sigma} - s_{\mathrm{m}}}{s_{\mathrm{th}}}\right)^{p}\right)^{q}\right], \tag{5}$$

where v_0 is a reference velocity, ΔF is an activation enthalpy for dislocation motion, k is Boltzmann's constant, θ is the absolute temperature, s_{m} is the resistance imposed by glide obstacles arising from the microstructure, and s_{th} is the intrinsic resistance of the material. The exponents p and q embody the effects of applied stress on reducing the activation enthalpy for glide. The microstructural resistance, s_{m}, is used to capture the collective effect of many features in the real microstructure by combining the strength contributions of the microstructural state variables we have chosen. Following Argon [15], we add contributions from obstacles that make local contact with the glide dislocations by summing their squares first and then taking the square root of the sum. Non-contact resistances, however, are superposed linearly. Certain obstacles provide both non-local and local contributions.

3. Components of microstructural resistance

3.1. Forest dislocations

A primary resistance experienced by glide dislocations in polycrystalline, fcc metals is due to the forest dislocation interactions. It leads to strain hardening and classically scales with the square root of the dislocation density. This local resistance takes the form

$$s_{\mathrm{d}} = M_{\mathrm{t}}\mu b\sqrt{\alpha\rho_{\mathrm{d}}}, \tag{6}$$

where M_{t} is the Taylor factor, μ is the shear modulus, and α is the dislocation junction strength parameter. For the present study, we consider this as the only contribution for the un-irradiated microstructure of the material.

3.2. Nanoscale prismatic dislocation loops

Each radioactive decay of a Pu nucleus results in the recoil of two energetic particles, a helium and a uranium nucleus. Each produces radiation damage, but U generates a particularly large collision cascade. Many of the interstitial and vacancy defects within the cascade aggregate immediately into clusters or small prismatic dislocation loops. The concentration of these loops increases with time, but reaches a saturation density after about two to three years in Pu alloys (citation). At this time, the continued generation of new loops is balanced by the disappearance of older loops due to thermal dissolution, migration to other defects, or recombination between interstitial- and vacancy-type defects.

Accordingly, the stress–strain behavior of the unirradiated material is modeled without the self-irradiation induced loop density while for all other simulations, the prismatic loop density was assumed to saturate in three years to a level of $N_{\mathrm{l}} = 3\times10^{23}\,\mathrm{m}^{-3}$ with a mean size of $d_{\mathrm{l}} = 1\,\mathrm{nm}$. While transmission electron microscopy investigations of aged Pu–Ga alloys have not revealed the dislocation loops, they are presumably either smaller than the resolution limit or less numerous than assumed for this study. If the later is true, our predictions will overestimate their contribution.

The small dislocation loops can be treated as point obstacles whose stress fields will exert a force on the gliding dislocations passing by at various distances. Detailed analyses of the loop-dislocation interactions have been carried out by Kroupa [16], Kroupa and Hirsch [17], Makin [18], and by Saxlova [19]. This interaction depends on the relative orientations of dislocation and loop, and their distance of closest approach. However, on average, the increase in the yield strength due to prismatic loops has been shown by comparison with experimental results to be consistent with

$$s_l = M_t \mu b \sqrt{\beta_l N_l d_l}, \tag{7}$$

where β_l is an empirical obstacle strength parameter [20].

Gliding dislocations may remove small dislocation loops resulting in obstacle-free channels [21] leading to a yield-drop phenomenon. Lacking clear evidence of a dominant presence of prismatic dislocation loops, however, we will neglect their removal during plastic deformation.

3.3. Helium bubbles

Helium atoms generated by the decay of Pu do not diffuse out of the material in any significant amount, but instead, accumulate in the form of small bubbles. Schwartz et al. [10] have recently acquired extensive microstructural data by TEM on the densities and size distributions of helium bubbles in Pu–Ga alloys of various ages. Fig. 1 shows a typical TEM image of He bubbles in a 42-year-old Pu–Ga alloy. The He bubbles have a number density of $\sim 2.05 \times 10^{23}\,\mathrm{m}^{-3}$ and an average diameter of 1.38 nm. The measured average bubble diameters and visible densities as a function of material age are shown in Fig. 2.

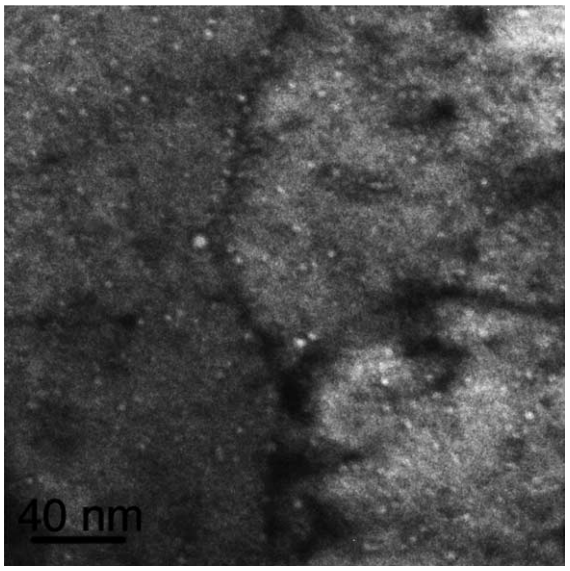

Fig. 1. Bright-field, under-focus Fresnel fringe image of He bubbles in a 42-year-old Pu–Ga alloy.

The nucleation and growth of helium bubbles during the continuous generation of helium from nuclear transmutations has been treated theoretically by Schaldach and Wolfer [22]. They showed that bubble nucleation is extremely rapid during the first year and then declines as the newly formed helium is captured more and more at existing bubbles. As a result, the helium remaining in solution becomes a negligible fraction of what is retained in bubbles. This theory has been used to fit the data shown in Fig. 2 in such a way as to slightly over-predict the total bubble density and under-predict the average

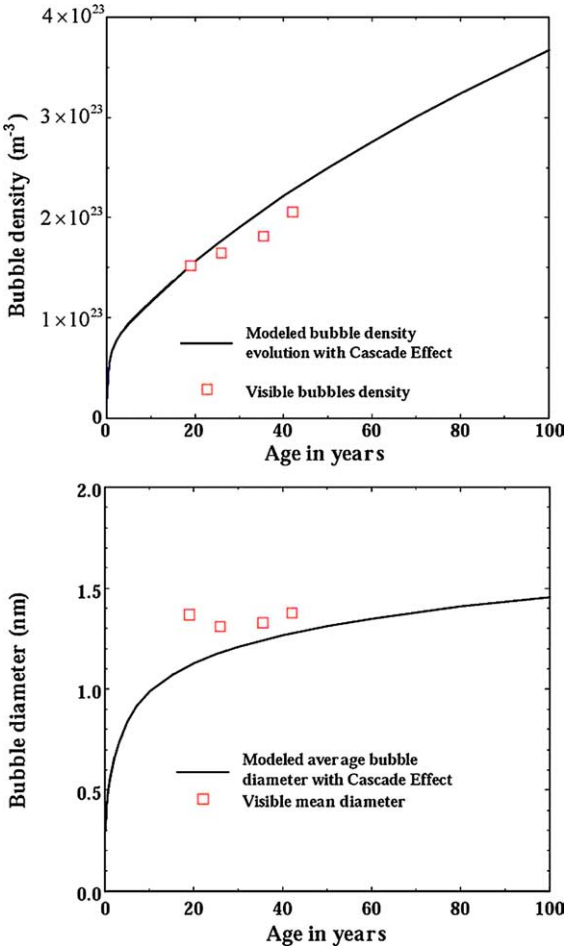

Fig. 2. Empirical measurements (squares) of bubble densities and diameters in aged plutonium (Schwartz et al. [10]) and model predictions (solid lines) of Schaldach and Wolfer [22]. The model lines overestimate the bubble density and underestimate the average bubble diameter based on the assumption that there is a density of helium bubbles with a size below the resolution limit of current electron microscopes.

bubble diameter accounting for small bubbles that are below the resolution limit of current electron microscopes. Both the TEM results as well as positron lifetime measurements of bubble containing samples indicate a helium density of 2–3 helium atoms per vacant lattice site within the bubbles.

The helium bubbles make three contributions to the glide resistance of dislocations. The first contribution accounts for the dislocation cutting through a bubble and creating a ledge, thereby increasing the surface area of the bubble. The increase in yield strength due to this effect can be derived from the cutting resistance of precipitate particles [15], and is given by

$$s_{\mathrm{b}} = M_{\mathrm{t}}\mu b\sqrt{\beta_{\mathrm{b}} N_{\mathrm{b}} R_{\mathrm{b}}}, \tag{8}$$

where β_{b} is the obstacle resistance of the helium bubble and is related to the surface energy of the bubble and shear modulus of the Pu–Ga alloy matrix.

The second contribution is due to the mismatch between elastic moduli inside the bubble and the surrounding solid. Willis et al. [24], and Gavazza and Barnett [25] were able to obtain closed form solutions for a straight screw dislocation in the vicinity of a spherical void. Using their void solution can be generally applied to bubbles because like the void, the bubble is assumed to have no effective shear modulus. However, their solutions are restricted to the dislocation never intersecting the cavity. The image interaction energy between a bubble and a straight screw dislocation is found to have an attractive, long-range behavior of $1/r^2$, where r is the shortest distance of the void center from the dislocation. When the dislocation intersects the void surface, the image interaction becomes about equal but opposite to the strain energy of the eliminated section of the dislocation, while the image interaction of the attached dislocation segments may be approximated by the maximum value of the above mentioned closed form solutions at $r = R$. Combining these results with the formalism of Gerold [26] for precipitation hardening, the following expression was derived for the resistance due to shear modulus misfit interactions of the helium bubble with the surrounding matrix:

$$s_{\mu} = \frac{1}{2} M_{\mathrm{t}}\mu b N_{\mathrm{b}} R_{\mathrm{b}}^2 \left[\ln\left(\frac{R_{\mathrm{b}}}{b}\right) + \frac{5(1-\nu)}{7-5\nu}\right], \tag{9}$$

where ν is the Poisson's ratio of the Pu–Ga alloy matrix.

The third contribution originates from the stress field of helium bubbles due to an imbalance between the gas pressure of the helium bubble and its surface tension. This effect is identical to one created by an over- or undersized spherical inclusion or precipitate, and accordingly, it is referred to as a misfit interaction or misfit strengthening in the precipitate hardening literature. Again using the formalism of Gerold [26], the following expression is derived for the resistance due to pressurized helium bubbles:

$$s_{\mathrm{P}} = \frac{3}{4} M_{\mathrm{t}} \left| P_{\mathrm{b}} - \frac{2\gamma_{\mathrm{b}}}{R_{\mathrm{b}}} \right|^{3/2} \sqrt{\frac{N_{\mathrm{b}}\pi}{2\mu b}} R_{\mathrm{b}}^2, \tag{10}$$

where P_{b} is the pressure of the helium in the bubble, and γ_{b} is the surface tension of the helium bubble.

The effect of all contributions on the dislocation glide resistance is now given by

$$s_{\mathrm{m}} = \sqrt{(s_{\mathrm{d}})^2 + (s_{\mathrm{l}})^2 + (s_{\mathrm{b}})^2} + s_{\mathrm{P}} + s_{\mu}, \tag{11}$$

where the contact interactions have been treated as aforementioned through a root sum square and the non-contact interactions have been linearly superposed. The model can be further augmented to include other material strengthening mechanisms not presently considered that may be uncovered in aged Pu–Ga alloys in the future.

4. Model behavior, baseline microstructure, and simulation results

The material strength and strain hardening/softening characteristics of the model can be analyzed through a set of closed form expressions. If the material is assumed to behave homogeneously under quasi-static loading conditions, then the effective plastic strain rate and temperature remain roughly constant after the material has begun to plastically deform. Analysis of the model under those conditions yields the following expression for the yield point of the material:

$$\sigma_y = \sqrt{(s_{\mathrm{d}})^2 + (s_{\mathrm{l}})^2 + (s_{\mathrm{b}})^2} + s_{\mathrm{P}} + s_{\mu} + s_{\mathrm{th}} \left\{ 1 - \left[\frac{k\theta}{\Delta F} \ln\left(\frac{\rho b v_0}{\dot{\bar{\varepsilon}}^{\mathrm{p}}} \right) \right]^{1/q} \right\}^{1/p}, \tag{12}$$

which looks similar to the form employed by Stout et al. [3]. As the number density of self-irradiation induced defects increases with aging the initial yield strength will increase and reflect those microstructural changes assuming that the aging process leaves the initial dislocation structure unaffected.

The constant strain rate and isothermal conditions also yield the following expression for the material point strain hardening/softening characteristics:

$$\frac{\mathrm{d}\bar{\sigma}}{\mathrm{d}\bar{\varepsilon}^{\mathrm{p}}} = \left(\frac{M_{\mathrm{t}}\mu b\alpha}{2\sqrt{\alpha\rho_{\mathrm{d}} + \beta_{\mathrm{l}} N_{\mathrm{l}} d_{\mathrm{l}} + \beta_{\mathrm{b}} N_{\mathrm{b}} R_{\mathrm{b}}}} - \frac{m}{\rho_{\mathrm{d}}} \right) \left(\frac{2}{b\bar{l}_{\mathrm{d}}} - \rho_{\mathrm{d}} \frac{R_{\mathrm{c}}}{2b} \right), \tag{13}$$

where m is given by the expression

$$m = \frac{s_{\text{th}} k\theta}{\Delta F p q}\left[1 - \left(\frac{\bar{\sigma} - s_{\text{m}}}{s_{\text{th}}}\right)^{\text{p}}\right]^{1-q}\left(\frac{\bar{\sigma} - s_{\text{m}}}{s_{\text{th}}}\right)^{1-p}. \quad (14)$$

The strain hardening/softening characteristics are more complex to analyze than the yield point characteristics; however, the expression in Eq. (13) shows that as the self-irradiation damage increases the strain hardening rate decreases. The dislocation density evolution has a less significant influence on the strength for highly irradiation damaged materials because it combines in the root-sum-squared expression with the irradiation-induced obstacles. Furthermore, while expression in the second set of parentheses is always positive, the expression in the first set of parentheses may become negative once a critical level of irradiation-induced defect densities is reached and material softening may appear.

The model was used to run a series of simulations to predict the mechanical behavior of δ-phase stabilized Pu–Ga alloys at different levels of accumulated self-irradiation damage. The material parameters associated with functional dependencies on Ga content, temperature, and strain rate were taken directly from Stout et al. [3]. The remaining material parameters that needed to be fit were associated with the strain hardening characteristics and material behavior changes associated with self-irradiation damage.

As previously mentioned, we evolved a dislocation density state variable to capture the strain hardening characteristics of the alloy whereas the MTS model of Stout et al. [3] evolved a strength state variable to capture the strain hardening characteristics. Due to the difference in the state variables, the material parameters associated with the strain hardening in model of Stout et al. could not be used directly. Instead, the material parameters associated with the dislocation density evolution and dislocation forest resistance were determined by fitting the unirradiated material behavior of our system to the behavior of the Stout model over the applicable span of temperatures and strain rates. The values of the material parameters determined from this procedure may be found in Appendix A.

The remaining material parameters associated with the irradiation damage effects on the mechanical strength were estimated from other published work. The prismatic loop obstacle strength was taken from experimental measurements of Dai et al. [20]. The surface energy of δ-Pu, γ_{b}, was estimated from empirical correlations [27], and the helium bubble obstacle strength was determined as a function of other known quantities following the work of Argon [15]. A list of values and formulas for the material parameters as a function of temperature and Ga content may be found in Appendix A.

The single material point simulations were run under conditions of ambient pressure, $\theta = 298\,\text{K}$, and $\dot{\varepsilon} = 1 \times 10^{-3}\,\text{s}^{-1}$. The Pu–Ga alloy simulated contained 2 wt% Ga, and an initial dislocation density of $\rho = 1 \times 10^{12}\,\text{m}^{-2}$ with an average segment length of 1 μm. In simulating the unirradiated material stress–strain behavior, the self-irradiation induced defect densities were assumed to be zero. For all other simulations, the prismatic loop density was assumed to saturate in three years to a level of $N_{\text{l}} = 3 \times 10^{23}\,\text{m}^{-3}$ with a mean size of $d_{\text{l}} = 1\,\text{nm}$. The helium bubble density and average size as a function of aging time were drawn from the predictions of the helium bubble evolution model of Schaldach and Wolfer [22]. The microstructural predictions, shown in Fig. 2, are used for the plasticity simulations in which the mechanical behavior of the alloy is plotted for alloy ages spanning one hundred years.

As previously stated, positron lifetime measurements of He bubbles in Pu indicate a possible He atom to Pu vacancy ratio between 2 and 3. Therefore, a series of simulations were run with three different He atom to Pu vacancy ratios: 2, 2.5 and 3. The results of the simulations are given in Figs. 3–5. A ratio of 2 leads to a He bubble pressure of $P_{\text{b}} = 0.8\,\text{GPa}$ while a ratio of 3 leads to pressure of $P_{\text{b}} = 5\,\text{GPa}$. At a ratio of 2 the He in the bubbles is most likely a liquid, while at a ratio of 3 the He in the bubbles is most likely a solid due to the packing density. While the state of the He in the bubbles in these alloys has not been experimentally confirmed, solid to liquid transitions have been observed in the He bubbles within other materials [28]. Of course, the assumptions inherent in the modulus misfit strength contribution would not be hold in the case of a solid He bubble, but we left contribution unchanged in this

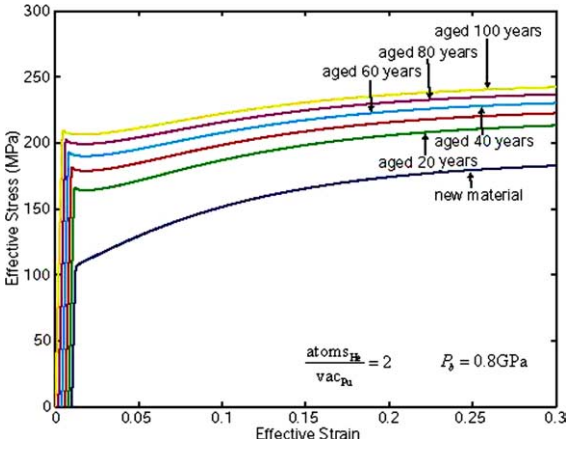

Fig. 3. Material point mechanical response predictions for a Pu–2%Ga alloy with different levels of self-irradiation damage due to aging. The helium bubble pressure was assumed to be 0.8 GPa corresponding to a He atom to Pu vacancy ratio of 2. The helium bubble densities and sizes corresponding the aging times shown were obtained from Fig. 2.

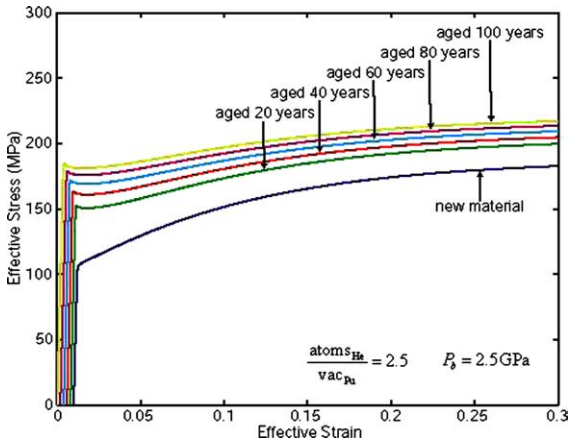

Fig. 4. Material point mechanical response predictions for a Pu–2%Ga alloy with different levels of self-irradiation damage due to aging. The helium bubble pressure was assumed to be 2 GPa corresponding to a He atom to Pu vacancy ratio of 2.5. The helium bubble densities and sizes corresponding the aging times shown were obtained from Fig. 2.

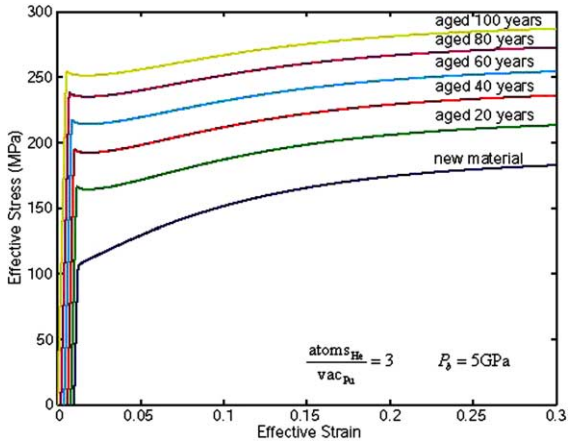

Fig. 5. Material point mechanical response predictions for a Pu–2%Ga alloy with different levels of self-irradiation damage due to aging. The helium bubble pressure was assumed to be 5 GPa corresponding to a He atom to Pu vacancy ratio of 3. The helium bubble densities and sizes corresponding the aging times shown were obtained from Fig. 2.

preliminary treatment to yield an upper bound as to the mechanical response at high He bubble pressures.

The series of stress strain curves in Figs. 3–5 show that the strength of the metal increases with the number of self-irradiation induced defects, while the strain hardening decreases. The stress strain response for all of the irradiated curves shows a slight initial softening at the onset of plasticity. For a He atom to Pu vacancy ratio of 2, the helium bubble pressure is significantly less than the surface tension force, and a significant contribution from s_P is observed. For a He atom to Pu vacancy ratio of 2.5, the helium bubble pressure is almost entirely offset by the surface tension of the helium bubble resulting in a small contribution from s_P. For a He atom to Pu vacancy ratio of 3, the helium bubble pressure is significantly greater than the surface tension force, and a significant contribution from s_P is regained. The s_P resistance appears to be sensitive to the helium pressure of the bubble for the range of He atom to Pu vacancy ratios that are consistent with current experimental observations [23].

Due to the initial strain softening in single material point simulations, the model would predict that the deformation behavior at yield of an aged Pu–Ga alloy tensile specimen would be inhomogeneous and lead to diffuse shear banding in the specimen. The engineering stress–strain response of a tensile specimen would most likely not exhibit the same softening due to the high strain rate sensitivity of the alloy. The single material point simulations were performed under constant strain rate conditions, and while such conditions could be enforced globally, locally the plastic strain rate in a shear band would be significantly higher than the macroscopic average value. Given the strong strain rate sensitivity of the material, tensile specimens would probably not exhibit the initial strain softening but rather exhibit an initial flat stress–strain response at low strains followed by moderate strain hardening at larger strains, similar to the behavior exhibited by polymers.

5. Conclusions

A constitutive model has been developed to predict the mechanical response of Pu–Ga alloys with significant levels of self-irradiation damage, including the presence of He bubbles. The alloys self-irradiate at a rate of 0.1 dpa per year and may accumulate significant amounts of damage in the form of small helium bubbles, prismatic dislocation loops, and other defects. The coarse-grained model presented here lumps all of the different defect microstructures into two self-irradiation induced defect densities with average defect sizes for both, and then uses these four microstructural parameters to establish a prediction for the stress strain response of aged Pu–Ga alloys for different levels of accumulated damage.

There is a significant amount of uncertainty that remains as to the level of damage that can be expected to accumulate with self-irradiation over the decades, and a significant amount of uncertainty as to the resultant mechanical behavior of these aged materials due to the lack of experimental observations. The predictions of the model developed here suggest that as the level of radiation damage increases the strength of the material should increase, while the strain hardening slope

should decrease. The plastic deformation mode of the material will remain typical of the unirradiated material but may eventually exhibit an increased tendency to flow localize as the level of damage increases. Strain softening behavior, as seen in other irradiated metals, is not expected due to the relatively high strain rate sensitivity of Pu–Ga alloys. Many of these predictions will be verified or refuted by measurements on specimens in the on-going accelerated aging program.

The predictions, however, are in qualitative agreement with mechanical property changes observed by Robinson [29] in AISI 316 stainless steels exposed to tritium gas. The β-decay of dissolved tritium resulted in helium accumulation in the steel without radiation damage. As in the case of plutonium, helium aggregated in bubbles with an average diameter of about 2 nm and bubble densities of $1\text{–}2.4\times10^{20}\,\mathrm{m}^{-3}$. Both the yield strength and the ultimate strength increased with helium accumulation in a manner qualitatively similar to these predictions. For the highest helium content of 535 appm, the yield strength had increased by 25%, while the ultimate strength had increased by 7%. Similar increases are predicted for the case shown in Fig. 4. Here, we assumed a helium density in the bubbles of 2.5 He atoms per vacant lattice site in δ-Pu. In stainless steels, this corresponds to a helium density of 1.2 He atom per vacant lattice site. Indeed, Robinson [29] had estimated a bubble density between 1.3 and 2.

Acknowledgments

This work was performed under the auspices of the US Department of Energy by University of California Lawrence Livermore National Laboratory under contract No. W-7405-Eng-48.

Appendix A

The following list of formulas was used to obtain the material parameter in the plasticity model. The majority of the formulas were obtained from Stout et al. [3]. The remainder was either fit to strain hardening behavior of that same model or developed from conjecture based on the behavior of other irradiated materials.

Material parameters obtained directly from Stout et al. [3]:

$$\mu = \left\{ 17\,366 + 2634\times(\mathrm{wt\%\,Ga}) + 5270\times\left[1-\exp\left(\frac{273\,\mathrm{K}}{\theta}\right)\right]^{-1}\right\}\mathrm{MPa},$$

$$b = 3.28\,\text{Å}, \qquad s_{\mathrm{th}} = 0.012025\times\mu,$$
$$\nu = 0.29, \qquad p = 0.5,$$
$$v_0 = 3.0488\times10^{4}\,\mathrm{m/s}, \qquad q = 1.5,$$
$$\Delta F = 0.7098\times\mu\times b^{3}, \qquad k = 1.38\times10^{-23}\,\mathrm{J/atom\text{-}K}.$$

Material parameters obtained by fitting the strain hardening behavior of this constitutive model to the hardening calculated using Stout et al. [3]:

$$\delta = 0.008, \qquad v_0 = 3.0488\times10^{4}\,\mathrm{m/s},$$
$$R_{\mathrm{c}} = \left\{10.59+\tfrac{\theta}{526\,\mathrm{K}}\right\}\mathrm{nm}, \qquad M_{\mathrm{t}} = 3.08,$$
$$\alpha = 0.08.$$

Material parameters chosen for the irradiation damage defect strength profile:

$$\beta_{\mathrm{i}} = 1\times10^{-3},$$
$$\gamma_{\mathrm{b}} = \left\{0.66+0.45\left(1-\frac{\theta}{913\,\mathrm{K}}\right)\right\}\mathrm{Pa\,m},$$
$$\beta_{\mathrm{b}} = 16\left(\frac{\gamma_{\mathrm{b}}}{\mu b}\right)^{3}.$$

References

[1] W. Wolfer, Los Alamos Sci. 38 (2000) 274.
[2] A. Arsenlis, B.D. Wirth, M. Rhee, Philos. Mag., in press.
[3] M.G. Stout, G.C. Kaschner, S.S. Hecker, LANL Report # LA-994458-PR, 2002.
[4] A. Seeger, in: Proceedings of the 2nd UN International Conference on Peaceful Uses of Atomic Energy, Geneva, United Nations, Vol. 6, 1958, p. 250.
[5] G.R. Odette, D. Frey, J. Nucl. Mater. 85&86 (1979) 817.
[6] S. Kojima, S.J. Zinkle, J. Nucl. Mater. 179–181 (1991) 982.
[7] G.E. Lucas, J. Nucl. Mater. 206 (1993) 287.
[8] A.M. Cuitiño, M. Ortiz, Model. Sim. Mater. Sci. Eng. 1 (1992) 225.
[9] A. Arsenlis, D.M. Parks, J. Mech. Phys. Solids 50 (2002) 1979.
[10] A.J. Schwartz, M.A. Wall, T. Zocco, C.M. Schaldach, W.G. Wolfer, Philos. Mag., in press.
[11] M.J. Caturla, M. Wall, E. Alonso, T. Diaz de la Rubia, T. Felter, M.J. Fluss, J. Nucl. Mater. 276 (2000) 186.
[12] G. Weber, L. Anand, Comp. Meth. Appl. Mech. Eng. 79 (1990) 173.
[13] U. Essmann, M. Rapp, Acta Metall. 21 (1973) 1305.
[14] A. Arsenlis, M. Tang, Model. Sim. Mater. Sci. Eng. 11 (2003) 265.
[15] A.S. Argon, in: R.W. Cahn, P. Haasen (Eds.), Physical Metallurgy, Vol. 4, Elsevier Science, 1996, Chapter 21.
[16] F. Kroupa, Philos. Mag. 7 (1962) 783.
[17] F. Kroupa, P.B. Hirsch, Discuss. Faraday Soc. 38 (1964) 49.
[18] M.J. Makin, Philos. Mag. 10 (1964) 695.
[19] M. Saxlova, Czech. J. Phys. B 19 (1969) 610.
[20] Y. Dai, D. Gavillet, F. Paschoud, M. Victoria, J. Nucl. Mater. 212–215 (1994) 393.

[21] J.S. Robach, I.M. Robertson, B.D. Wirth, A. Arsenlis, Philos. Mag. 83 (2003) 955.
[22] C.M. Schaldach, W.G. Wolfer, ASTM STP 1447, 2002.
[23] R.H. Howell, P.A. Sterne, J. Hartley, T.E. Cawan, Appl. Surf. Sci. 149 (1999) 103.
[24] J.R. Willis, M.R. Hayns, R. Bullough, Proc. R. Soc. Lond. A 329 (1972) 121.
[25] S.D. Gavazza, D.M. Barnett, Int. J. Eng. Sci. 12 (1974) 1025.
[26] V. Gerold, in: F.R.N. Nabarro (Ed.), Dislocations in Solids, Vol. 3, North-Holland, 1979, Chapter 15.
[27] L.E. Murr, Interfacial Phenomena in Metals and Alloys, Addison-Wesley, 1975, Chapter 3, p. 126.
[28] G.C. Abell, D.P. Cowgill, Phys. Rev. B 44 (1991) 4178.
[29] S.L. Robinson, Mater. Sci. Eng. 96 (1987) 7.